J. Fluid Mech. (1975), *vol.* 69, *part* 4, *pp.* 631–656
Printed in Great Britain

Numerical prediction of incompressible separation bubbles

By W. ROGER BRILEY AND HENRY McDONALD
United Technologies Research Center, East Hartford, Connecticut

(Received 5 August 1974)

A method is presented for performing detailed computations of thin incompressible separation bubbles on smooth surfaces. The analysis consists of finite-difference solutions to the time-dependent boundary-layer or Navier–Stokes equations for the flow in the immediate vicinity of the bubble. The method employs the McDonald–Fish turbulence model, to predict the development of the time-mean flow field, as influenced by the free-stream turbulence level. It also employs a viscous–inviscid interaction model, which accounts for the elliptic interaction between the shear layer and inviscid free stream. The numerical method is based on an alternating-direction implicit scheme for the vorticity equation. It employs transformations, to allow the free-stream boundary to change in time with the shape of the computed shear layer, and to ensure an adequate resolution of the sublayer region. Numerical solutions are presented for transitional bubbles on an NACA 66_3–018 airfoil at zero angle of incidence with chordal Reynolds numbers of $2{\cdot}0 \times 10^6$ and $1{\cdot}7 \times 10^6$. These have a qualitative behaviour similar to that observed in numerous experiments; they are also in reasonable quantitative agreement with available experimental data. Little difference is found between steady solutions of the boundary-layer and Navier–Stokes equations for these flow conditions. Numerical studies based on mesh refinement suggest that the well-known singularity at separation, which is present in conventional solutions of the steady boundary-layer equations when the free-stream velocity is specified, is effectively removed when viscous–inviscid interaction is allowed to influence the imposed velocity distribution.

1. Introduction

A technique is described herein for performing detailed computations of thin incompressible separation bubbles on smooth surfaces. Separation bubbles occur frequently on airfoils, especially downstream of the pressure peak near the leading edge of airfoils at incidence, and are known to influence the stalling characteristics of airfoils. Also, separation bubbles can be important in heat transfer applications, since experiments often reveal relatively low heat transfer in the separated region and relatively high heat transfer near reattachment. Three types of separation bubbles are distinguished here depending on where transition occurs. Bubbles are either laminar, transitional, or turbulent according to whether transition occurs far downstream of reattachment (if at all), between

separation and reattachment, or far upstream of separation, respectively. This terminology differs somewhat from that used in previous publications on airfoil separation bubbles (cf. Ward 1963), wherein the present transitional bubbles are referred to as laminar bubbles. Previous experimental work surveyed by Ward (1963) has also led to a distinction between 'short' and 'long' bubbles, although their effect on the pressure distribution is probably more important than their length. Short bubbles cover at most a few per cent of the airfoil chord and affect the pressure distribution only in the immediate vicinity of the bubble. Elsewhere, the pressure distribution is much the same as predicted by inviscid flow theory. Long bubbles cause a major change in the pressure distribution over the entire airfoil and can cover much of the airfoil surface. Only short bubbles are considered here, primarily because the analysis in its present form treats the interaction between bubble and inviscid flow by means of a localized correction to a specified inviscid pressure distribution. This restriction could be removed either by combining the present analysis with a time-dependent inviscid calculation procedure and allowing for interaction between the viscous and inviscid solutions, or for that matter by solving the Navier–Stokes equations for the entire flow field. While these approaches are in no way ruled out as possible alternatives to the present approach, they would at the very least require a substantial increase in computational effort to obtain a satisfactory resolution of the flow.

The present technique can be applied to completely laminar, transitional, or fully turbulent separation bubbles, although in view of the available experimental evidence and the authors' personal interests, only transitional bubbles are considered here. Most previous work on transitional separation bubbles has been experimental. It has focused on developing empirical correlations or semi-empirical theories for predicting what type of bubble (long or short) will occur in any given case, and what effect the bubble will have on the stalling characteristics of airfoils. Much of this work has been surveyed by Ward (1963). Recently, Crimi & Reeves (1972) and McCroskey & Philippe (1975) have combined semi-empirical theories for separation bubbles with inviscid flow theories and finite-difference calculation procedures for unsteady laminar and turbulent boundary layers, in efforts to predict dynamic stall. There does not appear to have been any previous attempt, however, to compute a transitional separation bubble in detail. Such an analysis is complicated by the presence of reverse flow, the effect of viscous–inviscid interaction, and the occurrence of transition in the separated shear layer. The present analysis is an outgrowth of the procedure used by Briley (1971) to compute laminar separation bubbles, and is based on a patching procedure wherein the time-dependent boundary-layer or Navier–Stokes equations are solved in the immediate vicinity of the bubble. The remainder of the flow field is treated using inviscid flow theory, and by solution of the steady boundary-layer equations. (See figure 1.) Such a patching procedure, based on boundary-layer theory, seems reasonable provided the separation bubble is of order $Re^{-\frac{1}{2}}$ in thickness and large-scale separation does not occur. Of course the patching approach presumes an adequate knowledge of boundary conditions at the interfaces. In addition to a viscous–inviscid interaction model,

the analysis employs the McDonald–Fish (1973) turbulence model, which was developed for transitional and turbulent boundary layers. The McDonald–Fish procedure is based on the solution of an integral form of the turbulence kinetic energy equation, to obtain the streamwise development of a one-parameter mixing-length profile normal to the wall. It allows for the influence of free-stream turbulence and wall roughness. Only minor modifications to the McDonald–Fish turbulence model were necessary for the application to transition in the separated shear layer. Although the McDonald–Fish turbulence model was well suited to implementation in the present computational scheme, it is emphasized that almost any of the currently available proven turbulence models (see, e.g., Launder & Spalding 1972) could be incorporated into the procedure, without significant change to any of the inferences to be made concerning the mathematical behaviour of the solutions. But the McDonald–Fish model does provide a realistic detailed description of the location of transition, and of mean flow behaviour during and after transition, including the sublayer region, as required by the present finite-difference solution procedure. Finally, although the present analysis is realistic only for relatively thin bubbles, it seems reasonable that the analysis might nevertheless serve as a useful element in a method for predicting the *onset* of large-scale separation. In fact, Shamroth & Kreskovsky (1974) have recently incorporated the present analysis into a procedure for computing time-dependent flow past airfoils, in an effort to predict the onset of dynamic stall.

2. Analysis

2.1. *Background*

2.1.1. *Viscous–inviscid interaction.* A division of the flow field into a viscous separation bubble region near the wall, and an inviscid outer region naturally gives rise to the possibility of viscous–inviscid interaction between the two regions, and consequently, to a change in the interface boundary conditions. In boundary-layer terminology, this would imply that the presence of the bubble changes the effective shape of the wall, which in turn alters the inviscid velocity or pressure distribution that would otherwise be imposed on the bubble. Of course, for flows involving large-scale separation such as occurs during stall, there is obviously very strong interaction. The bubble is no longer thin, and the boundary-layer concept is not applicable. There is substantial experimental evidence, however, that even relatively thin bubbles involve at least a localized interaction with the inviscid free stream (cf. Gault 1955; Gaster 1966).

Although most previous studies involving viscous–inviscid interaction have considered supersonic flow with separation, there have been several incompressible calculations, without interaction, involving either laminar separation or laminar separation bubbles. Efforts to solve the boundary-layer equations when there is separation have been complicated both by the need to account for downstream conditions after separation, and by an apparent singularity at the separation point. There is considerable analytical and numerical evidence that such a singularity exists when the steady boundary-layer equations are solved

in the conventional manner, with a specified free-stream velocity or pressure distribution (a *direct* solution). The separation singularity has been discussed, for example, by Goldstein (1948) and Brown & Stewartson (1969). The belief that the boundary-layer equations should nevertheless describe thin separation bubbles has led naturally to the hypothesis that the singularity results from a failure to allow in some manner for interaction with the inviscid flow. Since the usual separation singularity is manifested by an infinite displacement thickness and an infinite streamwise gradient of the wall shear at separation, efforts have been made to compute *inverse* solutions, in which a smooth displacement thickness or wall shear distribution is specified, and the free-stream velocity distribution obtained as part of the solution. There is some numerical evidence (Catherall & Mangler 1966; Klineberg & Steger 1974; Carter 1974) that this procedure removes the singularity at separation, although in some instances other difficulties have persisted downstream of separation. Regardless of whether displacement thickness or wall shear is specified, however, inverse solution procedures ultimately require some means for selecting boundary conditions that lead to a solution compatible with the inviscid free stream. Inverse procedures are therefore expected to be difficult to use routinely, inasmuch as they would require considerable skill on the part of the user, to determine the appropriate distribution of the specified variable that allows the desired free-stream conditions to be imposed. In any event, caution is necessary when numerical solutions are interpreted with regard to possible singularities. It will later be seen that it is possible to compute numerical solutions in which a singularity is locally smoothed away, even though it is presumably present in the exact differential solution. In this circumstance, a singularity can be detected only by mesh refinement.

Another problem which arises with the *steady* boundary-layer equations is that the spatial direction of integration changes locally with the direction of the streamwise velocity component. In a region of reverse flow, this implies that two solutions integrated from different directions must be compatible. Thus, even though the steady boundary-layer equations are parabolic everywhere, the separation bubble problem is not an initial-value problem, but requires downstream conditions after separation. Furthermore, if interaction with the inviscid free stream is allowed, this interaction is necessarily elliptic in character for subsonic flow.

2.1.2. *Previous work.* There have been numerous direct solutions, computed by forward-marching integration, that exhibit singular behaviour at separation. Catherall & Mangler (1966) first computed inverse solutions that are apparently regular at separation. Their procedure consisted of forward-marching integration with a smooth distribution of displacement thickness specified near separation. They nevertheless encountered a slight instability downstream of separation, which they attributed to a lack of uniqueness caused by the absence of downstream boundary conditions after separation.

In an effort to account properly for downstream boundary conditions, Briley (1971) solved the complete Navier–Stokes equations for the flow in the vicinity of thin laminar bubbles. This approach also avoided the separation singularity, since solutions of the Navier–Stokes equations are regular at separation. More

recently, Leal (1973) has computed solutions of the Navier–Stokes equations for steady separated flow over a flat plate in a linearly retarded free stream, in cases where the bubble is not thin. These solutions involve large-scale separation, and consequently a strong alteration of the pressure distribution over the entire plate from that which occurs for inviscid flow. Of particular interest are the direct solutions of the boundary-layer equations which Leal computed by forward-marching integration but using pressure distributions from his Navier–Stokes solutions. Although these boundary-layer solutions displayed singular behaviour at separation, the predicted location of the separation point approached that of the Navier–Stokes solutions as the Reynolds number was increased. Further Navier–Stokes solutions have been computed by Ghia & Davis (1974), to determine both the inviscid and viscous regions for flow past blunted semi-infinite thick plates, and including thin laminar bubbles.

Klemp & Acrivos (1972) devised a procedure for solving the steady boundary-layer equations, which accounts for downstream boundary conditions when there is reverse flow. They divided the boundary layer into two regions, along an assumed $u = 0$ curve, and computed direct solutions by forward-marching integration in the appropriate direction of the flow in each region. The assumed $u = 0$ curve was then adjusted iteratively, until the shear stress along this common boundary was continuous. Klemp & Acrivos applied their method to the problem of uniform flow past a parallel stationary flat plate of finite length, whose surface moves at constant velocity in a direction opposite to that of the free stream. It is not clear whether the Klemp–Acrivos procedure would be generally effective for other more conventional separated flows, however, since in the problem considered the separation and reattachment points are assumed known in advance, and separation is caused by a singularity in boundary conditions, rather than by an adverse pressure gradient.

Phillips & Ackerberg (1973) developed a method for solving the time-dependent boundary-layer equations when there is reverse flow. They computed solutions for flow past a semi-infinite flat plate parallel to a uniform free stream which fluctuates periodically in time, and incorporated downstream reverse-flow boundary conditions by using an exact Rayleigh solution. Although Phillips & Ackerberg encountered no singularity at the point of zero skin friction, there is apparently no evidence that a zero-skin-friction singularity exists for *unsteady* flow. It is therefore uncertain how the Phillips–Ackerberg method would behave in a computation involving steady separation.

Klineberg & Steger (1974) computed both direct and inverse numerical solutions for laminar separation bubbles, using a relaxation procedure for the steady boundary-layer equations. Of particular interest are their direct solutions of first-order accuracy which, with streamwise mesh refinement, display a singular behaviour at separation, despite a reasonable treatment of downstream conditions after separation. They were also able to compute second-order inverse solutions with specified wall shear stress, and these solutions are apparently regular at separation. One such case was presented in which the mesh was refined, however; and this appears to display singular behaviour in the computed pressure gradient and transverse velocity component downstream of separation.

Carter (1974) also computed inverse solutions for laminar bubbles, both with displacement thickness and with wall shear specified as a boundary condition.

2.1.3. *The present approach.* In the present analysis, the two-dimensional time-dependent form of both the Navier–Stokes equations and the boundary-layer equations are solved as an initial-value problem in time. The time-dependent approach greatly simplifies both the incorporation of downstream conditions after separation, and the treatment of interaction with an elliptic free stream. Steady solutions are obtained as the asymptotic limit for large time of the unsteady solution, in the same manner that steady flows are established physically. The time-dependent formulation therefore does not assume *a priori* the existence of a steady solution.

The analysis assumes that the bubble is thin enough for the boundary-layer concept to be valid; and the bubble solutions are computed with specified free-stream velocity distributions. But the particular velocity specified consists of the usual inviscid velocity plus an elliptic correction, which accounts for the viscous–inviscid interaction, and which is computed as part of the solution. Such solutions are aptly described as *interacted direct* solutions. The interacted bubble solution is thereby obtained using a single inviscid solution, which itself does not account for the interaction. This treatment of the interaction eliminates any need for iteration between several inviscid and boundary-layer solutions, in an effort to match boundary conditions. The interaction model assumes that the effective wall shape consists of the actual wall plus a thin correction, based on the distribution of displacement thickness in the localized interaction region. Although it is not established rigorously, numerical evidence based on mesh refinement will be presented which suggests that the interaction removes the separation singularity in the boundary-layer equations, without causing any subsequent difficulties in the separated flow region. Regardless of whether singularities are present in the exact *differential* solution, however, the numerical method used permits the computation of stable and smooth *difference* solutions, by using first-order difference approximations for streamwise derivatives. This locally smooths singularities in streamwise derivatives. Of course, the solutions would nevertheless approach the exact solution with mesh refinement, including any singularities which might be present. Computed results for transitional separation bubbles are compared with the experimental measurements of Gault (1955) and Bursnall & Loftin (1951). In general, good agreement is found.

2.2. *Governing equations*

2.2.1. *Basic equations.* The analysis begins with the time-averaged incompressible Navier–Stokes equations written in terms of vorticity and stream function. These are later reduced to the boundary-layer equations. Cartesian co-ordinates are appropriate, if surface curvature is assumed small in the region of the bubble. The time averaging is carried out in the usual manner for turbulent flows (e.g. Hinze 1959), by expressing the dependent variables as the sum of a time-averaged quantity (denoted by an overbar) and an instantaneous fluctuating quantity (denoted by a prime). The time averaging is performed over a

period of time sufficiently long to remove the random turbulent fluctuations, but not so long as to remove the time dependence of the mean flow. The two-dimensional time-averaged Navier–Stokes equations are given by

$$\frac{\partial\bar{\xi}}{\partial t}+\bar{u}\frac{\partial\bar{\xi}}{\partial x}+\bar{v}\frac{\partial\bar{\xi}}{\partial y}=\nu\left(\frac{\partial^2\bar{\xi}}{\partial x^2}+\frac{\partial^2\bar{\xi}}{\partial y^2}\right)-\frac{\partial^2\overline{u'v'}}{\partial y^2}+\frac{\partial^2\overline{u'v'}}{\partial x^2}-\frac{\partial^2(\overline{u'^2}-\overline{v'^2})}{\partial x\,\partial y}, \tag{2.1}$$

$$\bar{\xi}=\partial^2\bar{\psi}/\partial x^2+\partial^2\bar{\psi}/\partial y^2, \tag{2.2}$$

$$\bar{u}=\partial\bar{\psi}/\partial y,\quad \bar{v}=-\partial\bar{\psi}/\partial x. \tag{2.3}$$

ξ is vorticity; ψ is stream function; x and y are the streamwise and transverse co-ordinates; u and v are the x and y velocity components; ν is the (constant) kinematic viscosity; and t is time.

In view of the assumption of a thin shear layer, the Reynolds stress term $\partial^2\overline{u'v'}/\partial x^2$ is assumed small, and is neglected. Although the Reynolds normal stress term $\partial^2(\overline{u'^2}-\overline{v'^2})/\partial x\,\partial y$ is generally thought to be negligible in unseparated turbulent boundary layers, it is sometimes argued that this term acquires some importance near separation. Not much is available in the way of experimental measurements, however, to provide guidance in modelling this term in separation bubbles and during transition. The Reynolds normal stress term is therefore neglected in the vorticity equation, except in one instance, where it is retained for the purpose of evaluation. It is convenient for the analysis and consistent with the McDonald–Fish model to represent the turbulent stress $\overline{u'v'}$ in terms of an effective turbulent viscosity ν_T, where $\overline{u'v'}=-\nu_T\,\partial\bar{u}/\partial y$, and also to invoke the thin-shear-layer assumption, and set $\partial\bar{u}/\partial y\approx\bar{\xi}$ in this term. There are of course a number of physical shortcomings involved, as a result of using an effective viscosity hypothesis. As mentioned above, it is believed that these shortcomings would not influence the mathematical nature of the governing equations. Furthermore, alternative and less restrictive turbulence models can readily be incorporated into the present computational framework. In the case of the less restrictive models, however, the computational labour is usually greatly increased. The increased labour would be justifiable only by a potential improvement in predictive capability, not clearly evident at this time to the present authors.

It is important, for reasons of computational efficiency, to limit the extent of the computational domain in the y direction to the immediate vicinity of the shear layer. Since the thickness of the shear layer varies with x in a manner which is initially unknown, the following co-ordinate transformation is introduced:

$$\eta=y/h(x,t),\quad \tilde{x}=x,\quad \tilde{t}=t. \tag{2.4}$$

h, the physical location of the free-stream boundary, has a specified arbitrary shape which can vary with time. It is convenient to locate the free-stream boundary just outside the boundary layer; so h is defined by $h=1{\cdot}5\delta(x,t)$. (δ is the local boundary-layer thickness, defined as the point where $\bar{u}$ is 99 % of the free-stream velocity. It is computed from the numerical solution after each time step.) With this treatment, the shape of the outer boundary is adjusted with time, to fit the shape of the shear layer. The transformation (2.4) is incorporated

mathematically as a simple change in independent variables. Thus relative accelerations of Coriolis type arising from the moving co-ordinate system are neglected; but these terms are not significant for the present objective of computing steady solutions. After making the foregoing assumptions, and introducing the transformation (2.4), the tildes in (2.4) are dropped for notational simplicity. Equations (2.1)–(2.3) become

$$\frac{\partial \bar{\xi}}{\partial t}-\frac{\eta}{h}\frac{\partial h}{\partial t}\frac{\partial \bar{\xi}}{\partial \eta}+\bar{u}\frac{\partial \bar{\xi}}{\partial x}-\frac{1}{h}\frac{\partial \bar{\psi}}{\partial x}\frac{\partial \bar{\xi}}{\partial \eta}=\frac{1}{h^2}\left[\frac{\partial^2}{\partial \eta^2}(\nu+\nu_T)\bar{\xi}\right]+\nu D\bar{\xi}, \tag{2.5}$$

$$\bar{\xi}=(\partial^2\bar{\psi}/\partial\eta^2)/h^2+D\bar{\psi}, \tag{2.6}$$

$$\bar{u}=\frac{1}{h}\frac{\partial \bar{\psi}}{\partial \eta}, \quad \bar{v}=-\frac{\partial \bar{\psi}}{\partial x}+\frac{\eta}{h}\frac{\partial h}{\partial x}\frac{\partial \bar{\psi}}{\partial \eta}. \tag{2.7}$$

D denotes a differential operator defined by

$$D\equiv\frac{\partial^2}{\partial x^2}+\frac{\eta^2}{h^2}\left(\frac{\partial h}{\partial x}\right)^2\frac{\partial^2}{\partial \eta^2}+\frac{\eta}{h^2}\left[2\left(\frac{\partial h}{\partial x}\right)^2-h\left(\frac{\partial^2 h}{\partial x^2}\right)\right]\frac{\partial}{\partial \eta}-\frac{2\eta}{h}\left(\frac{\partial h}{\partial x}\right)\frac{\partial^2}{\partial x\,\partial \eta}. \tag{2.8}$$

With the stated assumptions for the turbulent Reynolds stresses, (2.5)–(2.8) represent the complete Navier–Stokes equations. However, these equations are reduced to a form which is equivalent to the boundary-layer equations, simply by neglecting the last term in each of (2.5) and (2.6), i.e. by defining $D\equiv 0$. Alternatively, this form of the boundary-layer equations can be obtained directly from their conventional velocity–pressure form by differentiation with respect to y and the definition $\bar{\xi}\equiv\partial\bar{u}/\partial y$.

The present analysis consists of a numerical solution of either the boundary-layer or Navier–Stokes form of (2.5)–(2.8). The wall and free-stream boundary conditions employed in the solution are

$$\bar{u}=\bar{v}=0 \quad \text{for} \quad \eta=0 \quad \text{and} \quad \bar{u}=\bar{u}_e+\bar{u}_I, \quad \bar{\xi}=0, \quad \text{for} \quad \eta=1. \tag{2.9}$$

$\bar{u}_e$ is the specified inviscid velocity distribution, and $\bar{u}_I$ is the elliptic correction due to viscous–inviscid interaction. It is a novel feature of the present analysis that both the location of the free-stream boundary h and the $\bar{u}_I$ portion of the free-stream boundary conditions are updated after each time step, and thereby evolve as part of the solution. At the upstream boundary, $\bar{\xi}$ and $\bar{\psi}$ profiles are prescribed from the output of a steady boundary-layer calculation procedure. In view of both its availability and compatibility with the present analysis, the McDonald & Fish (1973) procedure was used to compute the required steady boundary-layer solutions. At the downstream boundary, the conditions $\partial^2\bar{\xi}/\partial x^2=\partial^2\bar{\psi}/\partial x^2=0$ are good approximations for a thin boundary layer, and were employed when needed. If desired, the downstream velocity profiles computed from the present bubble analysis can be used to restart a steady boundary-layer calculation procedure, to complete the development of the reattached boundary layer (cf. figure 1). To complete the problem formulation, it remains to specify the effective turbulent viscosity ν_T and the interaction correction $\bar{u}_I$ in terms of the mean flow variables.

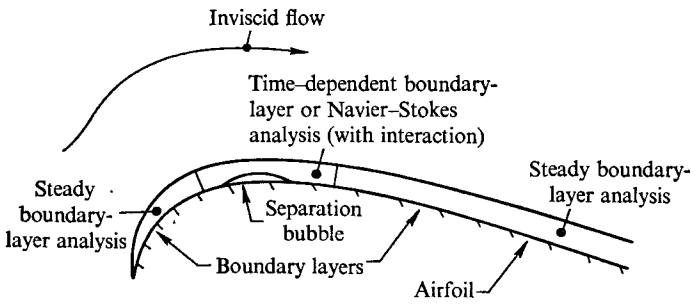

FIGURE 1. Schematic drawing of patching procedure for computing thin separation bubbles.

2.2.2. *Turbulence model.* Since the turbulence model used in the present calculations has been discussed in detail by McDonald & Fish (1973), only a brief summary is given here, along with a description of the modifications introduced for the application to separated flow. The turbulence model is based on the solution of an integral form of the turbulence kinetic energy equation. Following Townsend (1961) and Bradshaw, Ferriss & Atwell (1967), McDonald & Fish introduce structural scales a_n and L, together with a one-parameter mixing-length profile l. These scales are defined by

$$\left.\begin{aligned} |-\overline{u'v'}| &= a_1\overline{q^2}, \quad \overline{u'^2} = a_2\overline{q^2}, \quad \overline{v'^2} = a_3\overline{q^2}, \\ \epsilon &= |-\overline{u'v'}|^{\frac{3}{2}}/L, \quad -\overline{u'v'} = l^2|\partial\bar{u}/\partial y|\,\partial\bar{u}/\partial y. \end{aligned}\right\} \tag{2.10}$$

$\overline{q^2} = \overline{u'^2}+\overline{v'^2}+\overline{w'^2}$ is the turbulence kinetic energy, and ϵ represents the sum of the turbulence dissipation terms. Absolute values have been introduced, to accommodate negative turbulent shear stresses. Using the present notation, the incompressible form of the turbulence kinetic energy equation derived by McDonald & Fish (1973) can be written as

$$d(\phi_1 h)/dx = \phi_2 - \phi_3 + E, \tag{2.11}$$

where

$$\phi_1 = \int_0^{\delta/h} \frac{\bar{u}}{a_1}\left(\frac{l}{h}\frac{\partial\bar{u}}{\partial\eta}\right)^2 d\eta, \tag{2.12}$$

$$\phi_2 = \int_0^{\delta/h} 2\left(\frac{l}{h}\right)^2\left(1-\frac{l}{L}\right)\left|\frac{\partial\bar{u}}{\partial\eta}\right|^3 d\eta, \tag{2.13}$$

$$\phi_3 = \int_0^{\delta/h} 2h\left(\frac{a_2-a_3}{a_1}\right)\left(\frac{l}{h}\frac{\partial\bar{u}}{\partial\eta}\right)^2\left(\frac{\partial\bar{u}}{\partial x}-\frac{\eta}{h}\frac{\partial h}{\partial x}\frac{\partial\bar{u}}{\partial\eta}\right) d\eta, \tag{2.14}$$

$$E = \left[\overline{q^2}\left(\bar{u}\frac{\partial\delta}{\partial x}-\bar{v}\right)-2\overline{p'v'}\right]_e. \tag{2.15}$$

Since steady solutions are of primary interest in the present study, it is convenient to treat the turbulence as quasi-steady, and thus the steady form of the turbulence energy equation is solved at each time step. Solutions obtained using the present analysis, but based on the unsteady turbulence equation, are reported by Shamroth & Kreskovsky (1974). In (2.11) the ϕ_1 term represents the stream-

wise convection of turbulence energy, ϕ_2 represents the net production of turbulence, ϕ_3 represents the normal stress production, and E is a source term which represents the turbulence energy entrained from the free stream. Normally, E is dominated by the $\overline{q^2}$ term, and the pressure–velocity correlation $\overline{p'v'}$ can be neglected. For very small free-stream turbulence levels ($\overline{q^2}$ less than about 0·25%), however, the acoustic energy absorbed by the boundary layer can be important, and this energy contribution can be represented by the $\overline{p'v'}$ term in E.

The dissipation length scale L is obtained from an empirical fit to Bradshaw's (1967) measurements of L in an equilibrium boundary layer. It is given by

$$L = 0{\cdot}1\delta \tanh\left[\kappa y/(0{\cdot}1\delta)\right]. \tag{2.16}$$

κ is the von Kármán constant, taken as 0·43. On the basis of experimental evidence, the mixing length l is represented by a one-parameter (l_e) profile

$$l/\delta = (l_e/\delta)\tanh\left(\kappa y/l_e\right). \tag{2.17}$$

Both L and l are scaled by a sublayer damping factor $\mathscr{D}(y^+)$, where $y^+ = y(\tau/\rho)^{\frac{1}{2}}/\nu$, τ is shear stress, and ρ is density. The damping factor is given by

$$\mathscr{D} = P^{\frac{1}{2}}(y^+ - \overline{y^+})/\sigma. \tag{2.18}$$

P is the normal probability function, $\overline{y^+} = 23$ and $\sigma = 8$. In the present analysis, y^+ is based on a local stress; but, to accommodate negative shear stresses, absolute values are taken so that $\tau/\rho = (\nu + \nu_T)\,|\partial\bar{u}/\partial y|$, and the damping was not allowed to decrease in the positive y direction.

For fully turbulent boundary layers, the structural coefficient a_1 has a value of about 0·15. For transitional boundary layers, McDonald & Fish argue that a_1 is influenced mainly by viscosity, and accordingly set $a_1 = f(\bar{R}_\tau)$, where $\bar{R}_\tau$, the turbulence Reynolds number, is the layer-averaged value of ν_T/ν at a given streamwise location, i.e.

$$\bar{R}_\tau = \frac{1}{\delta}\int_0^\delta \nu_T\, dy/\nu. \tag{2.19}$$

The relationship between a_1 and $\bar{R}_\tau$ was derived from a consideration of the incompressible flat-plate equilibrium turbulent boundary layer. In terms of the momentum-thickness Reynolds number R_θ, a_1 is given by

$$a_1 = a_0(R_\theta/R_{\theta_0})/[1 + 6{\cdot}666a_0(R_\theta/R_{\theta_0} - 1)]. \tag{2.20}$$

a_0 is the value of a_1 at a specified Reynolds number R_{θ_0}. The change in independent variables from R_θ to $\bar{R}_\tau$ is accomplished with the empirical relationships

$$R_\theta = 68{\cdot}1\bar{R}_\tau + 614{\cdot}3, \quad \bar{R}_\tau > 40, \tag{2.21}$$

$$R_\theta = 100\bar{R}_\tau^{0{\cdot}22}, \quad \bar{R}_\tau \leqslant 1, \tag{2.22}$$

with a simple cubic interpolation (matching value and slope at the join points) for the intermediate zone $1 < \bar{R}_\tau < 40$. The constant a_0 has the value 0·012 at $\bar{R}_\tau = 1$. Solutions for attached boundary layers are not at all sensitive to the values of a_2 and a_3, and McDonald & Fish used the fully turbulent values of 0·5 and 0·2, respectively. The location of transition in the present bubble solutions, however, was more sensitive to the normal stress terms in (2.11), and hence to the value of $(a_2 - a_3)$; so these structural coefficients were given further con-

sideration. In the absence of any experimental evidence on the behaviour of (a_2-a_3) during transition, the assumption is made that (a_2-a_3) depends on $\bar{R}_\tau$, as does a_1. Klebanoff (1955) has measured turbulence characteristics in a fully turbulent flat-plate boundary layer: inside the sublayer, the measured value of $(\overline{u'^2}-\overline{v'^2})/\overline{q^2} = (a_2-a_3)$ increases from the fully turbulent value of 0·3 to a value of about 0·9 very near the wall, where the laminar viscosity is dominant (i.e. small $\bar{R}_\tau$). If it is assumed that the turbulence in the early stages of transition (small $\bar{R}_\tau$) has a structure similar to that in the viscous-dominated sublayer, then (a_2-a_3) should approach 0·9 for small $\bar{R}_\tau$. In the absence of any other evidence, (a_2-a_3) is approximated by the linear relationship

$$a_2-a_3 = \begin{cases} 0{\cdot}3+0{\cdot}6(1-\bar{R}_\tau), & \bar{R}_\tau < 1, \\ 0{\cdot}3, & \bar{R}_\tau \geqslant 1. \end{cases} \tag{2.23}$$

Given the relationships for the various structural scales and a knowledge of the mean flow, (2.11) becomes an ordinary differential equation which governs the streamwise development of the mixing-length parameter l_e. For fully turbulent equilibrium boundary layers, l_e/δ has a value near 0·09; for laminar flow, l_e/δ is zero. The only additional information necessary to determine transition is the free-stream turbulence level, which is seen to provide a small source term E in (2.11) which starts the transition process. After a two-point backward difference approximation is introduced for the x-derivative term, (2.11) provides an implicit integral relationship for l_e at x_j in terms of l_e at the previous upstream location x_{j-1}. This implicit relationship is easily solved by the standard secant method (Ralston 1965). Given the value of l_e that satisfies the turbulence energy equation, it is a simple matter to evaluate the turbulent viscosity ν_T from the mixing length.

2.2.3. *Viscous–inviscid interaction model.* The interaction model is based on the following assumptions: (i) the bubble is thin; (ii) the interaction region is localized, and coincides with the solution domain; and (iii) the interaction is due to the distribution of boundary-layer displacement thickness δ^* in the vicinity of the bubble. Accordingly, the effective wall shape is taken to be the actual wall plus a correction $\delta_I^*(x)$, the variation in δ^* from its value δ_0^* at the upstream boundary (the beginning of the interaction region). The definition of δ_I^* is shown schematically in figure 2. The surface correction δ_I^* is regarded as a 'thickness distribution', which occurs in a velocity field given by $\bar{u}_e(x)$, the inviscid velocity distribution appropriate for the actual (uncorrected) surface. With this interpretation of δ_I^* and the assumption that δ_I^* is thin, the interaction velocity correction $\bar{u}_I$ induced by δ_I^* can be evaluated using Allen's (1945) 'base profile' theory for thin airfoils. To implement Allen's theory, δ_I^* is replaced by a discrete source–sink system, one element of which is shown in figure 2. Each source–sink element $\Delta Q_{i+\frac{1}{2}}$ has a strength

$$\Delta Q_{i+\frac{1}{2}} = [(\delta_I^*)_{i+1}-(\delta_I^*)_i]\,\tfrac{1}{2}[(\bar{u}_e)_i+(\bar{u}_e)_{i+1}]. \tag{2.24}$$

At a given point x_m, the velocity induced by each source–sink element is $\Delta Q_{i+\frac{1}{2}}/2\pi(x_m-x_{i+\frac{1}{2}})$. The final velocity correction $\bar{u}_I$ at a given point is the sum of the velocities induced at this point by all of the source–sink elements in the interaction region. A minor difficulty, which arises with the assumption of a local

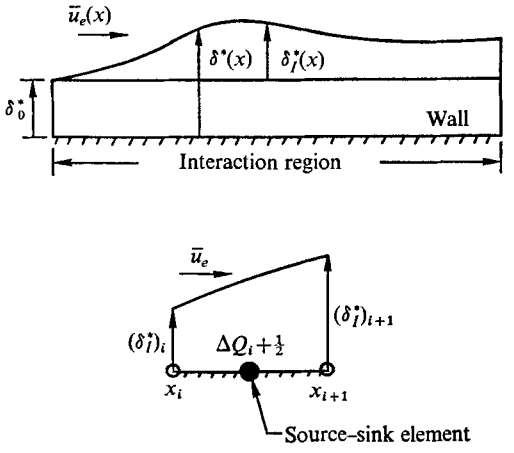

FIGURE 2. Schematic drawing of viscous–inviscid interaction model.

interaction region beginning at the upstream boundary, is that the interaction correction has its own 'leading-edge' region at the start of the interaction region. Consequently, the correction $\bar{u}_I$ is non-zero at the upstream boundary, and the corrected velocity distribution $\bar{u}_e + \bar{u}_I$ has a small jump at the upstream boundary. The small jump is removed by adding a constant amount to $\bar{u}_I$ at each point in the interaction region, to make $\bar{u}_I$ zero at the upstream boundary. The constant added to $\bar{u}_I$ represents an adjustment for the displacement or 'blockage' effect of the boundary layer upstream of the interaction region. The assumption that the interaction region is localized can of course be removed, if solutions are computed along the entire airfoil surface, rather than just in the immediate vicinity of the bubble.

2.3. *Method of solution*

2.3.1. *General features.* Solutions are computed for both the Navier–Stokes and boundary-layer forms of (2.5)–(2.7). In each case, the method of solution is based on an alternating-direction implicit (ADI) method for the vorticity equation (2.5). The discretization is carried out in the usual manner; and the notation $F^n_{i,j}$ is used to denote $F(x_i, \eta_j, t^n)$, where F is a surrogate symbol, representing any of the dependent variables. Although the transformation (2.4) improves computational efficiency by limiting the y extent of the solution domain to $0 \leqslant \eta \leqslant 1$, a further increase in efficiency is obtained by using a non-uniform mesh for η, so that grid points are very closely spaced in the sublayer region where gradients are very steep, and more widely spaced in the outer portion of the shear layer where gradients are much smaller. The analytical co-ordinate transformation of Roberts (1971) is a very effective means of introducing such a non-uniform mesh; it was employed in all computations reported here. If N grid points are to be used in the range $0 \leqslant \eta \leqslant 1$, then Roberts' transformation $\eta_T(\eta)$ is given by

$$\eta_T(\eta) = N + (N-1)\log\left(\frac{\eta+b-1}{\eta+b+1}\right)\Big/\log\left(\frac{b+1}{b-1}\right), \tag{2.25}$$

where $b = 1/(1-\eta_s)$, and η_s is a parameter equal to the estimated value of η at the edge of the sublayer region. The use of equally spaced points in the transformed co-ordinate η_T ensures an adequate resolution of both the overall region $0 \leqslant \eta \leqslant 1$ and the sublayer region $0 \leqslant \eta \leqslant \eta_s$.

If vorticity is regarded as the dependent variable, then (2.5) is linear if $\overline{u}$, $\partial\overline{\psi}/\partial x$, ν_T and h are known. Although each of these latter quantities ultimately depends on $\overline{\xi}$, they are lagged across a time step in the numerical computation of $\overline{\xi}$ (i.e. the lagged quantities are evaluated from the known solution at previous time levels, and updated after each time cycle). The vorticity equation (2.5) is approximated by an implicit two-point backward time-difference scheme; except as noted below, spatial derivatives are approximated by three-point, second-order central-difference formulae. In some circumstances, the use of central differences for convection terms can lead to instability, or other anomalous behaviour. In view of the enhanced stability it provides, the streamwise convection term $\overline{u}\,\partial\overline{\xi}/\partial x$ in (2.5) can, as an option, be approximated by the upwind difference scheme

$$\overline{u}\frac{\partial\overline{\xi}}{\partial x} \approx \begin{cases} \overline{u}_{i,j}(\overline{\xi}_{i,j} - \overline{\xi}_{i-1,j})/\Delta x, & \overline{u} \geqslant 0, \\ \overline{u}_{i,j}(\overline{\xi}_{i+1,j} - \overline{\xi}_{i,j})/\Delta x, & \overline{u} < 0. \end{cases} \tag{2.26}$$

This first-order differencing is equivalent to introducing a streamwise diffusion term with diffusion coefficient $\frac{1}{2}|\overline{u}|\,\Delta x$ (which therefore vanishes as Δx is decreased), and was used for all solutions presented here. But greater care is required for the transverse convection term $(\partial\overline{\psi}/\partial x)(\partial\overline{\xi}/\partial\eta)h$, since the transverse direction also includes physical diffusion terms that must be represented accurately. Second-order central differences are used for this transverse convection term; and no difficulty is anticipated, provided the transverse mesh spacing $\Delta\eta$ is sufficiently small. Difficulties may arise with the central difference formula, however, when the effective mesh Reynolds number $Re_{\Delta\eta} \equiv |\partial\overline{\psi}/\partial x|\,h\Delta\eta/(\nu+\nu_T)$ is greater than two (cf. Roache 1972). In the outer portion of the shear layer, where both $\partial\overline{\psi}/\partial x$ and $\Delta\eta$ are relatively large, $Re_{\Delta\eta}$ was sometimes greater than two for the mesh spacings used. In this circumstance, small η-direction spatial oscillations in $\overline{\xi}$ developed near the outer boundary, and instability followed. The instability was apparently due to the sensitivity of the computed boundary-layer thickness δ, and hence of the outer boundary location h, to these oscillations. It was found that the oscillations could be eliminated via the computational stratagem of not allowing the total viscosity $\nu+\nu_T$ to have a value less than $\frac{1}{2}|\partial\overline{\psi}/\partial x|\,h\Delta\eta$ *outside the boundary layer* (i.e. for $y \geqslant \delta$), thereby ensuring that $Re_{\Delta\eta}$ is no greater than two in this region. But second-order accuracy is rigorously maintained inside the boundary layer; and, although the viscous shearing stress term has only first-order accuracy outside the boundary layer, the shearing stress is very small in this region; consequently, the increased smoothing outside the boundary layer is not believed to introduce any significant error. The error in the computed solutions will later be examined by mesh refinement.

2.3.2. *Navier–Stokes procedure.* The procedure for solving the Navier–Stokes form of (2.5)–(2.8) employs the ADI technique of Douglas & Gunn (1964), to solve the backward time-difference approximation for the vorticity equation

(2.5). It is similar to the procedure used by Briley (1971), except for the treatment of vorticity boundary conditions at the wall. In the present method, the condition $\bar{v} = 0$ at the wall is satisfied by setting $\bar{\psi}_{i,w} = 0$, where the subscript w denotes the wall value of j. The vorticity–stream-function relation (2.6) then reduces to $\bar{\xi}_{i,w} = (\partial^2\bar{\psi}/\partial\eta^2)_{i,w}/h_i^2$ at the wall, and the approximation of this latter formula by central differences introduces the quantity $\bar{\psi}_{i,w-1}$, which in turn is eliminated using a central difference approximation for the no-slip condition,

$$\bar{u}_{i,w} = (\partial\bar{\psi}/\partial\eta)_{i,w}/h_i = 0.$$

The final vorticity boundary condition has second-order accuracy. It is given by

$$\bar{\xi}_{i,w}^{n+1} = 2(d\eta_T/d\eta)_w^2\,\bar{\psi}_{i,w+1}^{n+1}/(h_i\Delta\eta_T)^2. \tag{2.27}$$

$\Delta\eta_T$ is the (uniform) grid spacing in the transformed co-ordinate η_T. Equation (2.27) couples the vorticity and stream-function solutions; and, since the solution procedure requires implicit boundary values for vorticity before the stream function is available, the wall condition (2.27) is satisfied iteratively. In the solution procedure, the backward time-difference form of the vorticity equation (2.5) is solved by the Douglas & Gunn (1964) ADI procedure for parabolic equations, in which the x-direction and then the η-direction derivatives of $\bar{\xi}$ are treated implicitly in successive steps, and the resultant linear difference approximations for $\bar{\xi}^{n+1}$ are solved by a simple tridiagonal-matrix technique. The difference form of the stream-function equation (2.6) is solved iteratively, using the Peaceman & Rachford (1955) ADI method for elliptic equations. Since the implicit treatment of the cross-derivative term appearing in the differential operator D is awkward for ADI methods, this term is treated explicitly (i.e. evaluated from known quantities at the n level) in both of (2.5) and (2.6). The iterative procedure for satisfying the vorticity boundary condition (2.27) is based on a point-to-point application of the well-known secant method (cf. Ralston 1965), to obtain values of $\bar{\xi}_{i,w}^{n+1}$ and $\bar{\psi}_{i,w+1}^{n+1}$ that satisfy (2.27). Using two different sets of assumed values for wall vorticity, denoted by f_i^1 and f_i^2, (2.5) and (2.6) are solved by the procedures outlined above, to obtain $\bar{\xi}^{n+1}$ and $\bar{\psi}^{n+1}$ at interior points, and two sets of errors are recorded: E_i^1 and E_i^2, which are defined as the difference between the assumed values of wall vorticity and those computed from (2.27). The third and successive guesses for wall vorticity at each streamwise location are obtained from the secant-method iteration formula

$$f_i^q = f_i^{q-1} + E_i^{q-1}(f_i^{q-1} - f_i^{q-2})/(E_i^{q-2} - E_i^{q-1}), \quad q = 3, 4, \ldots. \tag{2.28}$$

q is the iteration index. It is convenient to use values of wall vorticity from the previous time step, $\bar{\xi}_{i,w}^n$, as the initial guess f_i^1, and to obtain f_i^2 by adding a small constant to f_i^1. Since the initial guess $\bar{\xi}_{i,w}^n$ is a very good approximation to the final solution $\bar{\xi}_{i,w}^{n+1}$, the secant method normally converges after only one application of (2.28). In the flow cases considered here, the foregoing solution procedure was found to be stable for time steps at least 50 times the maximum time step permitted by the viscous stability criterion

$$\Delta t \leqslant \min_{i,j}[(\Delta\eta)^2/2(\nu + \nu_T)h^2], \tag{2.29}$$

which would be applicable to many explicit methods.

2.3.3. *Boundary-layer procedure.* The solution procedure for the boundary-layer equations is the same as that described for the Navier–Stokes equations, except for a major simplification which is possible, since the stream-function equation (2.6) contains no x derivatives when $D \equiv 0$ and is therefore a one-dimensional equation relating $\overline{\psi}$ to $\overline{\xi}$. Being one-dimensional, the central difference approximation to (2.6) can be combined with the η-direction-implicit step of the ADI solution procedure for the vorticity equation. The resultant linear system of equations for $\overline{\xi}^{n+1}$ and $\overline{\psi}^{n+1}$ along an η-direction row of grid points can be written in block-tridiagonal form, and solved by standard block-elimination techniques. (See Isaacson & Keller 1966.) The advantage of this procedure is that the wall boundary condition (2.27), which couples $\overline{\xi}^{n+1}_{i,w}$ and $\overline{\psi}^{n+1}_{i,w+1}$, can be included in the block-tridiagonal system and solved without iteration. Two costly iteration procedures required for solution of the Navier–Stokes equations are thereby eliminated in the solution of the boundary-layer equations: (i) the elliptic ADI iteration for the stream-function equation; and (ii) the secant iteration for wall vorticity. Consequently, the overall solution procedure for the boundary-layer form of the governing equations required only about one half to one third of the computational effort per time step required by the complete Navier–Stokes equations.

3. Results

3.1. *Computed solutions and comparisons with experiment*

Solutions are presented here for transitional bubbles occurring on an NACA 66_3-018 symmetric airfoil at zero angle of incidence. The first case considered was computed for comparison with the experimental measurements of Gault (1955), made using an airfoil with 5 ft chord and at a Reynolds number Re_c of 2×10^6 and free-stream turbulence level Tu of 0·15–0·2 %. These parameters are defined by $Re_c = \overline{u}_\infty c/\nu$ and $Tu = 100(\overline{q^2}/3)^{\frac{1}{2}}/\overline{u}_\infty$, where $\overline{u}_\infty$ is the velocity of the uniform flow at large distance from the airfoil, and c is the chord length. The only additional information required by the analysis is the inviscid velocity distribution $\overline{u}_e$ over the airfoil; this was obtained from Gault's measurements. Gault measured the pressure distribution for several Reynolds numbers in the range $1{\cdot}5 \times 10^6$ to 1×10^7; at the highest Reynolds number, transition occurred upstream of what would have been the laminar separation point; consequently, there was no separation bubble, and no evidence of viscous–inviscid interaction due to a bubble. The pressure distribution data at $Re_c = 1 \times 10^7$ were therefore fitted with a curve, and used as the inviscid pressure distribution for the airfoil. This pressure distribution was used to specify the inviscid velocity distribution $\overline{u}_e$ for the case at $Re_c = 2 \times 10^6$, which does have a bubble and the associated interaction.

It will be shown subsequently that, for the range of flow parameters under consideration, there is very little difference between solutions computed for the boundary-layer and Navier–Stokes form of the governing equations. Therefore, all solutions presented are for the boundary-layer form of the equations, except where otherwise noted. The first solution presented here has $Re_c = 2 \times 10^6$, $Tu = 0{\cdot}175$ %. It was computed with 31×55 grid points for the η and x direc-

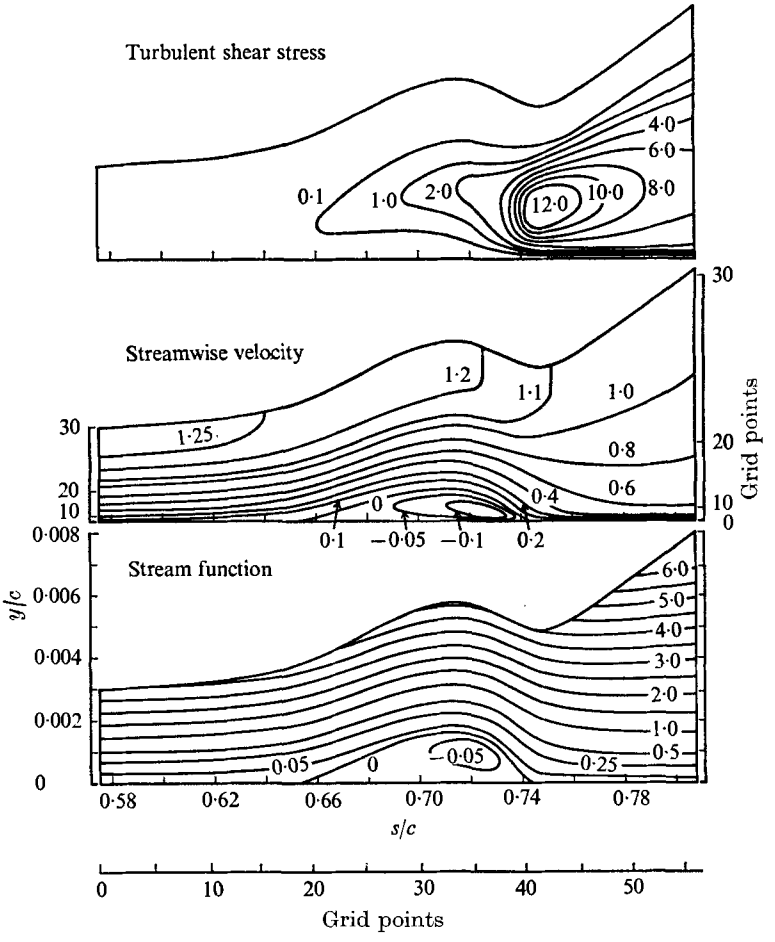

FIGURE 3. Contour plots: turbulent shear stress $(2\overline{u'v'}/\bar{u}_\infty^2) \times 10^3$; streamwise velocity $\bar{u}/\bar{u}_\infty$; stream function $(\bar{\psi}/\bar{u}_\infty c) \times 10^3$. $Re_c = 2 \times 10^6$, $Tu = 0{\cdot}175\,\%$, 31×55 grid.

tions, respectively. Contour plots for this bubble solution are shown in figure 3, where both the transverse distance y and arc length s along the airfoil are normalized by the chord. The separation and reattachment points are apparent from the stream-function and velocity contours; the bubble length is approximately 9 % of the chord. The region in which transition occurs is clearly visible in the contours of turbulent shear stress; and the development of a turbulent boundary-layer structure, with laminar sublayer downstream of reattachment, is evident in the contours of $\bar{u}$. The separated region consists of relatively stagnant flow just downstream of separation, with a more vigorous vortex motion near reattachment. A strikingly similar structure for the flow in transitional bubbles has been observed experimentally by Gaster (1966) and Young & Horton (1966). The streamwise development of various boundary-layer parameters is shown in figure 4. The parameters have the following definitions: pressure coefficient $c_p = 1 - (\bar{u}_e/\bar{u}_\infty)^2$; skin friction $c_f = 2\nu(\partial\bar{u}/\partial y)_w/\bar{u}_e^2$; displacement thickness

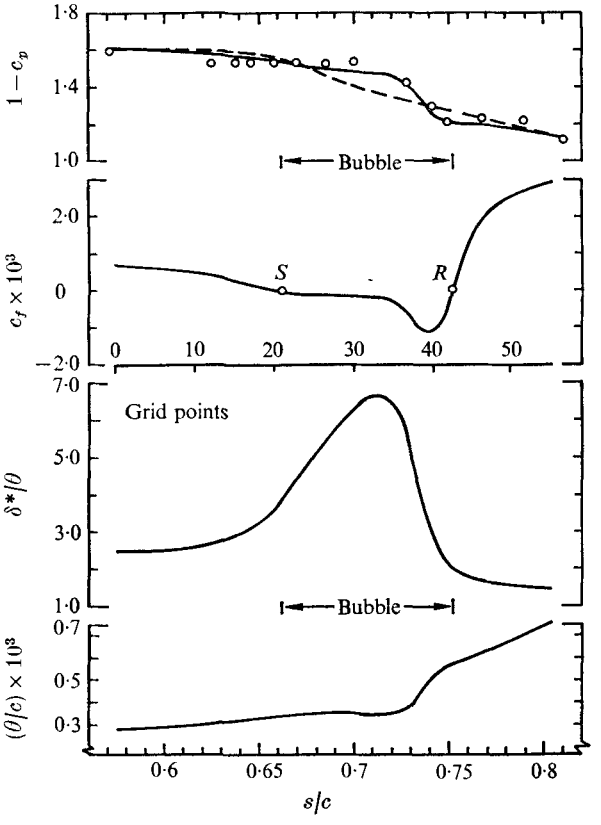

FIGURE 4. Boundary-layer parameters: pressure distribution $1-c_p$, skin friction c_f, shape factor δ^*/θ, momentum thickness θ/c against streamwise distance s/c. $Re_c = 2 \times 10^6$, $Tu = 0{\cdot}175\,\%$, 31×55 grid.

$\delta^* = \int_0^\delta (1-\bar{u}/\bar{u}_e)\,dy$; momentum thickness $\theta = \int_0^\delta (1-\bar{u}/\bar{u}_e)(\bar{u}/\bar{u}_e)\,dy$. The computed pressure distribution, which includes the correction for viscous–inviscid interaction, has a relatively constant pressure region downstream of separation, and rapidly returns to the specified inviscid pressure distribution near reattachment. The computed pressure distribution is in good agreement with Gault's (1955) experimental measurements, which are also shown in figure 4. A similar qualitative behaviour for the pressure distribution near separation bubbles has been observed in numerous other experiments, in particular Gaster (1966). The relatively stagnant flow downstream of separation, and the more intense vortex motion near reattachment, are again evident in the computed skin-friction curve. Velocity profiles at selected streamwise locations are shown in figure 5, and are generally in excellent agreement with Gault's experimental measurements. The maximum reverse flow computed inside the bubble is approximately 13 % of the local free-stream velocity.

A second case was computed for the same NACA 66_3-018 airfoil for comparison with the earlier measurements of Bursnall & Loftin (1951) for $Re_c = 1{\cdot}7 \times 10^6$ and

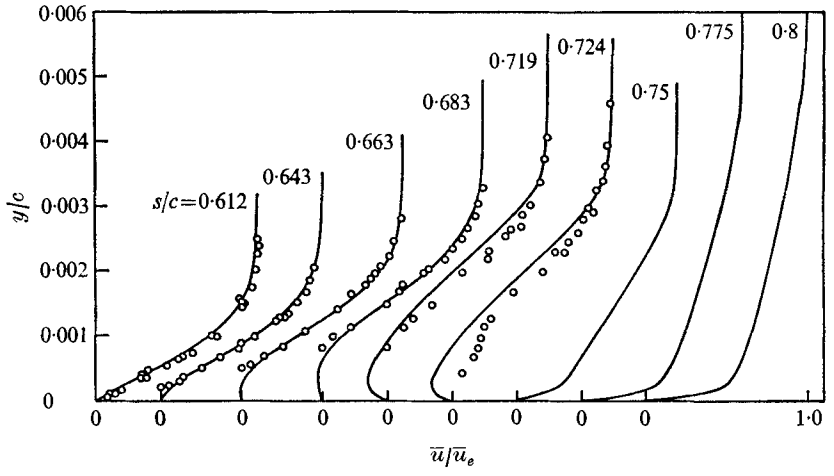

FIGURE 5. Streamwise velocity $\bar{u}/\bar{u}_e$ against transverse distance y/c, at selected streamwise locations s/c: ——, computed, $Tu = 0{\cdot}175\,\%$; ○, measurements of Gault (1955), $Tu = 0{\cdot}15$–$0{\cdot}2\,\%$. $Re_c = 2 \times 10^6$, 31×55 grid.

a free-stream turbulence level quoted as a few hundredths of a per cent. A high Reynolds number pressure distribution without separation was not available for this case, so the pressure distribution measured by Bursnall & Loftin for $Re_c = 1{\cdot}7 \times 10^6$ was employed, but this measured (interacted) pressure distribution was modified near the bubble, to remove the characteristic 'bump' caused by bubble interaction. It is noted, however, that the measured pressure distribution has a maximum value of about 1·8 for $(1 - c_p)$, which disagrees with the value of about 1·6 measured by Gault and indicated by inviscid flow theory (Abbott & von Doenhoff 1959). Concerning the free-stream turbulence level, it has been observed experimentally (cf. McDonald & Fish 1973) that the location of transition as measured in different wind tunnels becomes insensitive to free-stream turbulence for very small turbulence levels, say Tu less than $0{\cdot}25\,\%$. A plausible explanation is that transition is then dominated not by the free-stream vorticity fluctuations, but by the acoustic energy absorbed by the boundary layer. For the purpose of prediction, it would therefore be unrealistic to evaluate the E term in the turbulence energy equation on the basis of a free-stream turbulence level of a few hundredths of a per cent, as quoted by Bursnall & Loftin, for almost certainly transition in this case was precipitated by a largely unknown disturbance probably acoustic in origin. The value $0{\cdot}2\,\%$ for Tu was therefore used in the numerical prediction, since this value led to approximate agreement between the computed and measured location of transition. It may be noted in passing that the present authors' interests lie largely in the flow regime dominated by large free-stream vorticity fluctuations. Computed velocity profiles for this case are compared with Bursnall & Loftin's measurements in figure 6. The agreement is regarded as reasonable, except near reattachment, where the streamwise grid spacing is considered inadequate to resolve fully the very rapid flow variations observed experimentally.

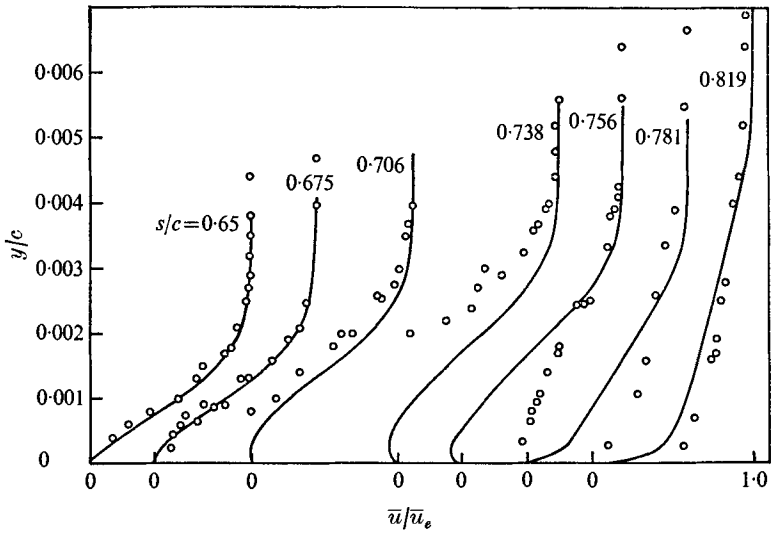

FIGURE 6. Streamwise velocity $\bar{u}/\bar{u}_e$ against transverse distance y/c, at selected streamwise locations s/c: ——, computed; ○, measurements of Bursnall & Loftin (1951). $Re_c = 1{\cdot}7 \times 10^6$, $Tu = 0{\cdot}2\,\%$.

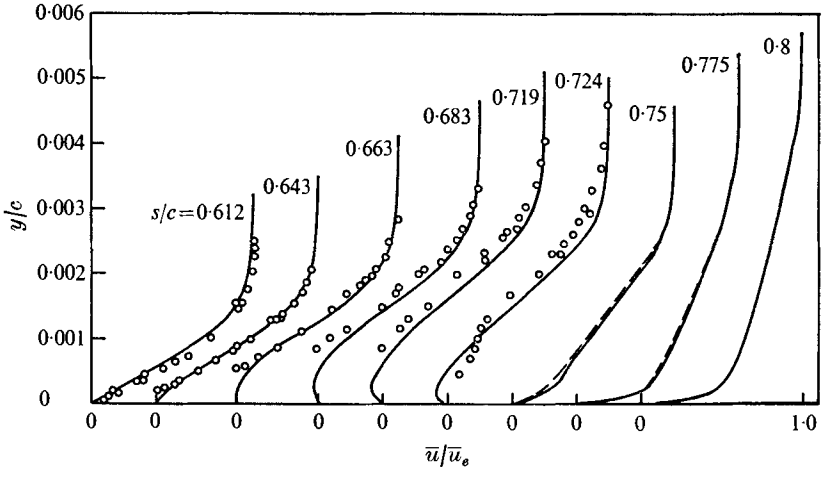

FIGURE 7. Streamwise velocity $\bar{u}/\bar{u}_e$ against transverse distance y/c, at selected streamwise locations s/c: ——, computed, boundary layer; – – –, computed, Navier–Stokes; ○, measurements of Gault (1955). $Re_c = 2 \times 10^6$, $Tu = 0{\cdot}175\,\%$, 31×28 grid.

3.2. *Comparison with Navier–Stokes solutions*

Using a 31×28 grid, solutions of both the boundary-layer and Navier–Stokes forms of the equations were computed, using the same boundary conditions, for the Gault case with $Re_c = 2{\cdot}0 \times 10^6$ and $Tu = 0{\cdot}175\,\%$. Velocity profiles from these two solutions are shown in figure 7; it can be seen that there is very little difference between the boundary-layer and Navier–Stokes solutions. The differences may well reflect purely numerical errors, due to differences in the various convergence criteria used in the two numerical methods. The general implications

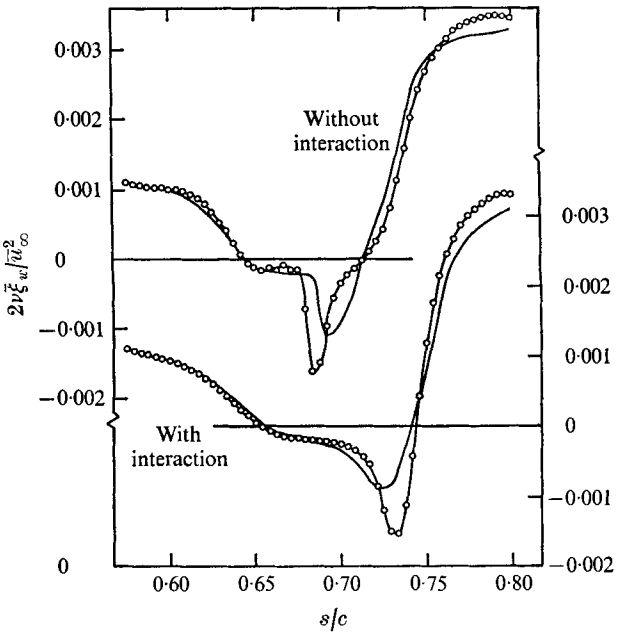

FIGURE 8. Mesh refinement: wall shearing stress $2\nu\bar{\zeta}_w/\bar{u}_\infty^2$ against streamwise distance s/c. ——, 31×28 grid; —○—, 31×55 grid. $Re_c = 2 \times 10^6$, $Tu = 0{\cdot}175\,\%$.

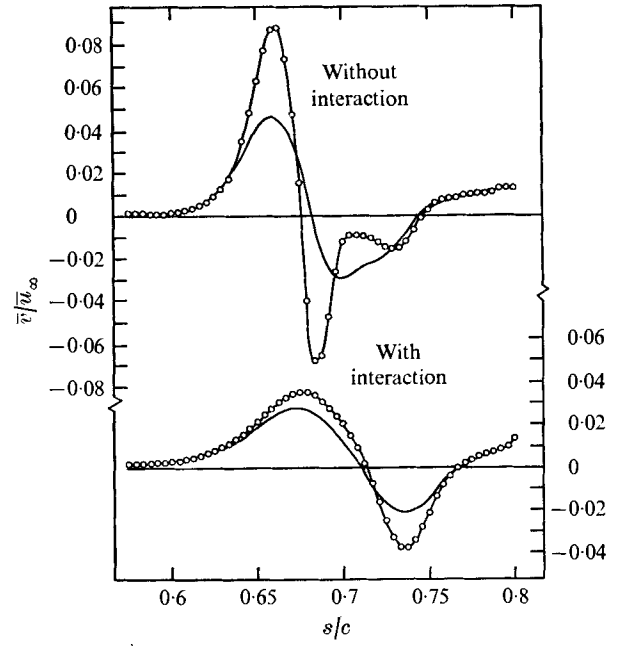

FIGURE 9. Mesh refinement: transverse velocity at outer boundary $\bar{v}/\bar{u}_\infty$ against streamwise distance s/c. ——, 31×28 grid; —○—, 31×55 grid. $Re_c = 2 \times 10^6$, $Tu = 0{\cdot}175\,\%$.

of this comparison are not without some ambiguity, since only one set of flow conditions is considered, and since it must be assumed that the imposed free-stream boundary conditions represent an adequate treatment of the patching interface. Furthermore, even in the case considered, differences may exist between the boundary-layer and Navier–Stokes solutions that are not resolved for this particular choice of grid spacing. Nevertheless, the comparison in figure 7 does suggest that the boundary-layer equations are adequate to describe the behaviour of thin separation bubbles. Consequently, no further solutions of the Navier–Stokes equations are presented herein.

3.3. *Effect of viscous–inviscid interaction*

The effect of interaction on the solutions was examined by recomputing bubble solutions without interaction (i.e. setting $\bar{u}_I = 0$), using Gault's measured pressure distribution for $Re = 1 \times 10^7$, and using both 31×55 and 31×28 grids. The wall shearing stress and the transverse velocity component $\bar{v}$ at the outer boundary ($\eta = 1$) from these solutions are shown in figures 8 and 9; they are compared with similar results from the corresponding interacted solutions. The non-interactive solutions display a somewhat erratic behaviour in the region of the bubble when the streamwise mesh is halved. In particular, the shear stress undergoes an abrupt change downstream of separation, and the transverse velocity shows signs of becoming singular. This behaviour is not surprising, in view of the previously mentioned evidence that a separation singularity exists in solutions of the boundary-layer equations when the free-stream velocity is specified without allowing for interaction. The singularity is presumably smoothed over a few grid points by the first-order differencing for the x direction. The interactive solutions in figures 8 and 9 have a more reasonable dependence on the mesh spacing than the non-interactive solutions, particularly near separation; these interactive solutions *appear* to be regular at separation. If any singularities are present in the exact differential solution, they are at the very least considerably weakened by the interaction. Further evidence of the validity of the interactive solutions near separation is provided by the agreement with experiment shown previously. The only area of potential difficulty in the interactive solutions when the mesh is refined appears to be near reattachment, where the vortex motion associated with reattachment gives rise to relatively large negative shear stresses. The variation with streamwise grid spacing of the wall shear distribution, just upstream of reattachment in figure 8, can be interpreted either as evidence of some sort of singularity, or simply as truncation error in a region where the solution varies rapidly with streamwise distance because of the intense vortex motion near reattachment. Although no firm conclusion can be reached on the basis of the results in figures 8 and 9, the authors are inclined to favour the latter interpretation for two reasons. The first is that the intense vortex motion is in qualitative agreement with experimental observations from several sources (e.g. Gaster 1966; Young & Horton 1966; references therein). Second, in the particular flow being computed, Gault's (1955) measurements indicate that the entire reattachment process, as evidenced by the measured

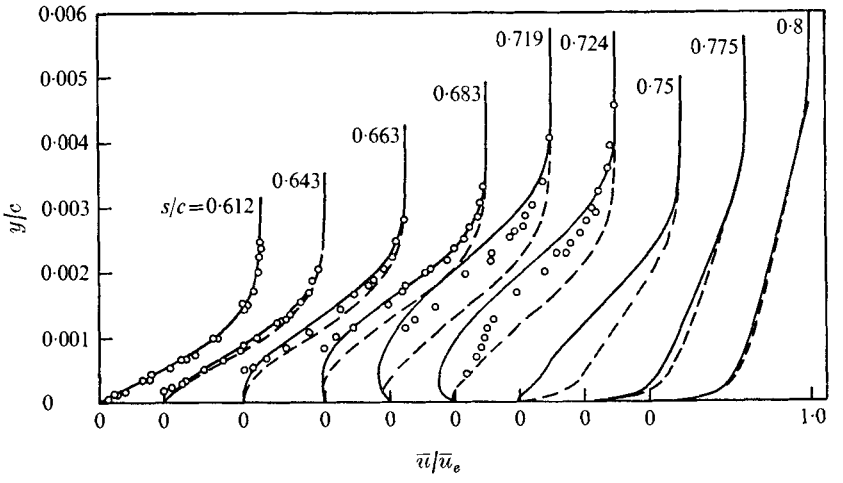

FIGURE 10. Streamwise velocity $\bar{u}/\bar{u}_e$ against transverse distance y/c, at selected streamwise locations s/c: ——, computed, Tu = 0·2 %; – – –, computed, Tu = 0·15 %; ○, measurements of Gault (1955), Tu = 0·15–0·2 %. $Re_c = 2 \times 10^6$, 31 × 28 grid.

velocity profiles, takes place in a very short streamwise distance (approximately 1–2 % of the chord). The smallest mesh spacing used in the present solutions (31 × 55 grid) corresponds to a streamwise mesh spacing of about 0·4 % of the chord; and the predicted reattachment process occurs over about 3 % of the chord in this solution. This is consistent with the possibility that the flow near reattachment is not fully resolved by the 31 × 55 grid. Of course, if streamwise gradients were to become sufficiently large near reattachment, this would again bring into question the validity of the boundary-layer approximations for this region.

3.4. *Further comparisons*

In figure 10, solutions computed with the same 31 × 28 grid, but with free-stream turbulence levels Tu of 0·15 % and 0·2 %, are shown. As would be expected, the effect of the higher free-stream turbulence level is to move the transition point upstream, and consequently, to reduce the size of the bubble. As shown in figure 10, the computed velocity profiles are somewhat sensitive to the free-stream turbulence level, at least in the region of the bubble where transition occurs. There is much less difference between the computed profiles at the downstream boundary s/c = 0·8, where the flow is fully turbulent.

A summary of the effect that various changes in the solution procedure have on the computed wall shearing stress relative to a reference case with a 31 × 28 grid is shown in figure 11. As mentioned previously, the effect of an increase in free-stream turbulence Tu from 0·15 % to 0·2 % is to move the transition point upstream, thereby reducing the size of the bubble, as is evident in figure 11. An increase in the number of transverse grid points from 31 to 41 is seen to have very little effect on the computed wall shear. This lack of dependence on transverse mesh spacing is an indication that numerical truncation errors are small for the transverse direction. The difference between the boundary-layer and Navier–

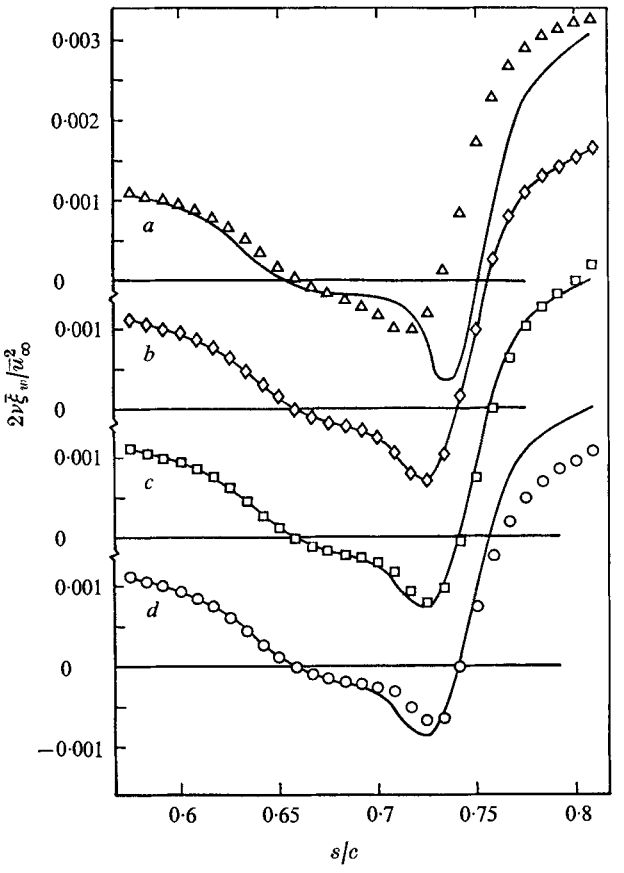

FIGURE 11. Wall shearing stress $2\nu\bar{\xi}_w/\bar{u}_\infty^2$ against streamwise distance s/c: (*a*) △, $Tu = 0{\cdot}2\,\%$; ——, $Tu = 0{\cdot}15\,\%$. (*b*) ◇, 41×28 grid; ——, 31×28 grid. (*c*) □, Navier–Stokes; ——, boundary layer. (*d*) ○, with normal stress; ——, without normal stress. $Re_c = 2 \times 10^6$.

Stokes solutions is also included in figure 11; as mentioned previously, this difference is relatively minor, and possibly due to numerical error. The effect of including the turbulent normal stress terms in the time-averaged vorticity equation is also shown in figure 11. The normal stress terms were modelled in the same manner as in the turbulence kinetic energy equation, i.e. the last term in (2.1) was replaced by

$$-\frac{\partial^2(\overline{u'^2}-\overline{v'^2})}{\partial x\,\partial y} \doteq -\frac{\partial^2}{\partial x\,\partial y}\left[\frac{(a_2-a_3)}{a_1}\nu_T\left|\frac{\partial\bar{u}}{\partial y}\right|\right], \tag{3.1}$$

and treated explicitly in the numerical solution procedure. Although the normal stress terms do have some effect on the solution, including them did not affect the location of transition. Thus the influence of the normal stress terms is not regarded as highly significant. The transient behaviour of wall shearing stress, at selected streamwise locations, is shown in figure 12 for a typical solution. These transients are included as a demonstration that the computed solutions were indeed steady; the degree of accuracy of the transients in figure 12 was not

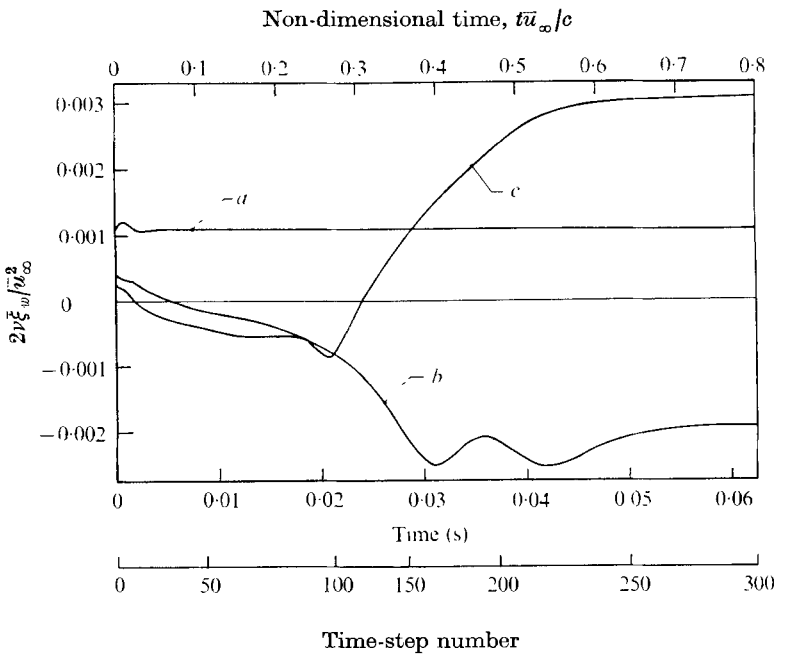

FIGURE 12. Wall shearing stress $2\nu\bar{\xi}_w/\bar{u}_\infty^2$ against time at selected streamwise locations: (*a*) $s/c = 0{\cdot}579$, near upstream boundary; (*b*) $s/c = 0{\cdot}725$, maximum negative shear; (*c*) $s/c = 0{\cdot}8$, near downstream boundary. $Re_c = 2 \times 10^6$, $Tu = 0{\cdot}175\,\%$, 31×55 grid.

established. Finally, although not shown here, solutions for attached transitional boundary layers computed with the present method were found to be in excellent agreement with corresponding solutions computed by the McDonald & Fish (1973) procedure. Additional comparisons between computations made with the present procedure and analytic solutions are presented by Shamroth & Kreskovsky (1974).

Since the numerical method is implicit, and therefore not subject to conventional explicit stability limits, the same time step can be used with different spatial mesh sizes. As a consequence, the computer time required for a given solution is approximately linear in the number of spatial grid points. A typical case with a 31×55 grid required about 300 time steps to reach steady state (cf. figure 12) and about 20 min of UNIVAC 1110 computer time. About one half of the computational effort was spent evaluating the turbulence model; about one quarter was spent solving the implicit difference equations. The relative amount of computer time spent evaluating the turbulence model is considerable. But presumably it is less than might result from solving a number of partial differential equations, as would perhaps be required for one of the more recent multi-equation turbulence models. Consequently, it would seem prudent to explore fully the potential of the simpler models, such as the present one, prior to embarking on the considerable labour of a multi-equation model.

4. Conclusions

(i) A method has been developed which is suitable for making routine and economical detailed computations of thin incompressible separation bubbles on smooth surfaces. The method requires as input only the inviscid velocity distribution along the surface and the free-stream turbulence level. The method accounts for interaction with the inviscid free stream; but it does not require an elaborate iterative scheme for matching viscous and inviscid boundary conditions. The method also provides a realistic detailed description of the location of transition and of mean flow behaviour during and after transition, including the sublayer region.

(ii) Computed solutions for transitional separation bubbles on an airfoil were found to be in reasonable agreement, both qualitatively and quantitatively, with available experimental data.

(iii) When the same boundary conditions were used, little difference was found between steady solutions of the boundary-layer and Navier–Stokes equations in a test case consisting of a thin bubble at high Reynolds number.

(iv) Numerical evidence was obtained, which suggests that the well-known separation singularity, present in conventional solutions of the steady boundary-layer equations when the free-stream velocity is specified, is effectively removed when viscous–inviscid interaction is allowed to influence the imposed velocity distribution.

REFERENCES

ABBOTT, I. H. & VON DOENHOFF, A. E. 1959 *Theory of Wing Sections*. Dover.

ALLEN, H. J. 1945 General theory of airfoil sections having arbitrary shape or pressure distribution. *N.A.C.A. Rep.* no. 833.

BRADSHAW, P. 1967 The turbulence structure of equilibrium boundary layers. *J. Fluid Mech.* **29**, 625.

BRADSHAW, P., FERRISS, D. J. & ATWELL, N. P. 1967 Calculation of boundary-layer development using the turbulent energy equation. *J. Fluid Mech.* **28**, 593.

BRILEY, W. R. 1971 A numerical study of laminar separation bubbles using the Navier–Stokes equations. *J. Fluid Mech.* **47**, 713.

BROWN, S. N. & STEWARTSON, K. 1969 Laminar separation. In *Annual Review of Fluid Mechanics*, vol. 1. Palo Alto, California: Annual Reviews Inc.

BURSNALL, W. J. & LOFTIN, L. K. 1951 Experimental investigation of localized regions of laminar boundary-layer separation. *N.A.C.A. Tech. Note*, 2338.

CARTER, J. E. 1974 Solutions for laminar boundary layers with separation and reattachment. *A.I.A.A. Paper*, no. 74-583.

CATHERALL, D. & MANGLER, K. W. 1966 The integration of the two-dimensional laminar boundary-layer equations past the point of vanishing skin friction. *J. Fluid Mech.* **26**, 163.

CRIMI, P. & REEVES, B. L. 1972 A method for analyzing dynamic stall. *A.I.A.A. Paper*, no. 72-37.

DOUGLAS, J. & GUNN, J. E. 1964 A general formulation of alternating direction methods. *Numerische Mathematik*, **6**, 428.

GASTER, M. 1966 The structure and behaviour of laminar separation bubbles. *Separated Flows, Part* 2, *AGARD Conf. Proc.* no. 4, p. 819. London: Technical Editing and Reproduction, Ltd.

GAULT, D. E. 1955 An experimental investigation of regions of separated laminar flow. *N.A.C.A. Tech. Note*, no. 3505.

GHIA, U. & DAVIS, R. T. 1974 Navier–Stokes solutions for flow past a class of two-dimensional semi-infinite bodies. *A.I.A.A. J.* **12**, 1659.

GOLDSTEIN, S. 1948 On laminar boundary layer flow near a position of separation. *Quart. J. Mech. Appl. Math.* **1**, 43.

HINZE, J. O. 1959 *Turbulence*. New York: McGraw-Hill.

ISAACSON, E. & KELLER, H. B. 1966 *Analysis of Numerical Methods*. Wiley.

KLEBANOFF, P. S. 1955 Characteristics of turbulence in a boundary layer with zero pressure gradient. *N.A.C.A. Rep.* no. 1247.

KLEMP, J. B. & ACRIVOS, A. 1972 A method for integrating the boundary-layer equations through a region of reverse flow. *J. Fluid Mech.* **53**, 177.

KLINEBERG, J. M. & STEGER, J. L. 1974 On laminar boundary layer separation. *A.I.A.A. Paper*, no. 74–94.

LAUNDER, B. E. & SPALDING, D. B. 1972 *Mathematical Models of Turbulence*. Academic.

LEAL, L. G. 1973 Steady separated flow in a linearly decelerated free stream. *J. Fluid Mech.* **59**, 513.

MCCROSKEY, W. J. & PHILIPPE, J. J. 1975 Unsteady viscous flow on oscillating airfoils. *A.I.A.A. J.* **13**, 71.

MCDONALD, H. & FISH, R. W. 1973 Practical calculations of transitional boundary layers. *Int. J. Heat Mass Transfer*, **16**, 1729.

PEACEMAN, D. W. & RACHFORD, H. H. 1955 The numerical solution of parabolic and elliptic differential equations. *J. Soc. Ind. Appl. Math.* **3**, 28.

PHILLIPS, J. H. & ACKERBERG, R. C. 1973 A numerical method for integrating the unsteady boundary-layer equations when there are regions of backflow. *J. Fluid Mech.* **58**, 561.

RALSTON, A. 1965 *A First Course in Numerical Analysis*. McGraw-Hill.

ROACHE, P. J. 1972 On artificial viscosity. *J. Comp. Phys.* **10**, 169.

ROBERTS, G. O. 1971 Computational meshes for boundary layer problems. *Proc. 2nd Int. Conf. on Numerical Methods in Fluid Dynamics*, p. 171. Springer.

SHAMROTH, S. J. & KRESKOVSKY, J. P. 1974 A weak interaction study of the viscous flow about oscillating airfoils. *N.A.S.A. Rep.* CR-132425.

TOWNSEND, A. A. 1961 Equilibrium layers and wall turbulence. *J. Fluid Mech.* **11**, 97.

WARD, J. H. 1963 The behaviour and effects of laminar separation bubbles on aerofoils in incompressible flow. *J. Roy. Aero. Soc.* **67**, 783.

YOUNG, A. D. & HORTON, H. P. 1966 Some results of investigations of separation bubbles. *Separated Flows, Part* 2, *AGARD Conf. Proc.* no. 4, p. 785. London: Technical Editing and Reproduction, Ltd.